In Vitro Evaluation and Mitigation of Niclosamide's Liabilities as a COVID-19 Treatment.

Jesse W. Wotring[1], Sean M. McCarty[1], Khadija Shafiq[1], Charles J. Zhang[1], Theophilus Nguyen[2], Sophia R. Meyer[1], Reid Fursmidt[2], Carmen Mirabelli[3], Martin C. Clasby[1], Christiane E. Wobus[3], Matthew J. O'Meara[4], Jonathan Z. Sexton[1,2,5] *

[1] Department of Medicinal Chemistry, College of Pharmacy, University of Michigan, Ann Arbor, MI, 48109, USA.

[2]Department of Internal Medicine, Gastroenterology and Hepatology, Michigan Medicine at the University of Michigan, Ann Arbor, MI, 48109, USA.

[3]Department of Microbiology and Immunology, University of Michigan, Ann Arbor, MI, USA.

[4]Department of Computational Medicine and Bioinformatics, University of Michigan, Ann Arbor, MI 48109, USA.

[5]U-M Center for Drug Repurposing, University of Michigan, Ann Arbor, MI, 48109, USA.

* Corresponding author: jzsexton@med.umich.edu

1

Abstract

Niclosamide, an FDA-approved oral anthelmintic drug, has broad biological activity including anticancer, antibacterial, and antiviral properties. Niclosamide has also been identified as a potent inhibitor of SARS-CoV-2 infection *in vitro,* generating interest in its use for the treatment or prevention of COVID-19. Unfortunately, there are several potential issues with using niclosamide for COVID-19, including low bioavailability, significant polypharmacology, high cellular toxicity, and unknown efficacy against emerging SARS-CoV-2 variants of concern. In this study, we used high-content imaging-based immunofluorescence assays in two different cell models to assess these limitations and evaluate the potential for using niclosamide as a COVID-19 antiviral. We show that despite promising preliminary reports, the antiviral efficacy of niclosamide overlaps with its cytotoxicity giving it a poor *in vitro* selectivity index for anti-SARS-CoV-2 inhibition. We also show that niclosamide has significantly variable potency against the different SARS-CoV-2 variants of concern and is most potent against variants with enhanced cell-to-cell spread including B.1.1.7. Finally, we report the activity of 33 niclosamide analogs, several of which have reduced cytotoxicity and increased potency relative to niclosamide. A preliminary structure-activity relationship analysis reveals dependence on a protonophore for antiviral efficacy, which implicates nonspecific endolysosomal neutralization as a dominant mechanism of action. Further single-cell morphological profiling suggests niclosamide also inhibits viral entry and cell-to-cell spread by syncytia. Altogether, our results suggest that niclosamide is not an ideal candidate for the treatment of COVID-19, but that there is potential for developing improved analogs with higher clinical translational potential in the future.

Key Words: Niclosamide, SARS-CoV-2, COVID-19, Polypharmacology, Drug Repurposing

Importance

There is still an urgent need for effective anti-SARS-CoV-2 therapeutics due to waning vaccine efficacy, the emergence of variants of concern, and limited efficacy of existing antivirals. One potential therapeutic option is niclosamide, an FDA approved anthelmintic compound that has shown promising anti-SARS-CoV-2 activity in cell-based assays. Unfortunately, there are significant barriers for the clinical utility of niclosamide as a COVID-19 therapeutic. Our work emphasizes these limitations by showing that niclosamide has high cytotoxicity at antiviral concentrations, variable potency against variants of concern, and significant polypharmacology as a result of its activity as a nonspecific protonophore. Some of these clinical limitations can be mitigated, however, through structural modifications to the niclosamide scaffold, which we demonstrate through a preliminary structure activity relationship analysis. Overall, we show that niclosamide is not a suitable candidate for the treatment of COVID-19, but that structural analogs with improved drug properties may have higher clinical-translational potential.

Introduction

Since it emerged as a novel betacoronavirus in late 2019, Severe Acute Respiratory Syndrome Coronavirus 2 (SARS-CoV-2) has caused a global pandemic[1]. COVID-19, the disease caused by SARS-CoV-2 infection, presents as varying symptoms with different degrees of severity ranging from dry cough and difficulty breathing to acute cardiac injury and refractory pulmonary failure[2,3]. As of April 2022, COVID-19 has caused the death of over six million individuals worldwide[4] and this death toll continues to increase as new SARS-CoV-2 Variants of Concern (VOCs) emerge with enhanced transmissibility and increased adaptive immune escape[5].

74   The deadly impact of COVID-19 has created a need to identify potential antiviral treatments for

75   SARS-CoV-2 infection. This has culminated in the development and FDA-

76   authorization/approval of several vaccines[6], and three small-molecule antiviral medications

77   including remdesivir[7], molnupiravir[8], and Paxlovid[9]. Unfortunately, because of limited

78   worldwide vaccine availability[10], the modest clinical efficacy of existing antivirals[8,9,11,12], and the

79   potential resistance of SARS-CoV-2 variants[13,14], additional therapeutics are urgently needed to

80   help stop the spread of the virus.

81   A promising strategy for identifying new therapies with the potential for rapid deployment is

82   drug repurposing, whereby compounds with already established safety profiles and robust supply

83   chains are used to treat other diseases[15]. Since the start of the pandemic, several large-scale drug

84   repurposing screens have been conducted[16–20] and have identified many different potential

85   candidates for the treatment of COVID-19. One of the repurposed drugs, which had potent anti-

86   SARS-CoV-2 efficacy *in vitro,* was the oral anthelmintic compound niclosamide[17,20].

87   Traditionally used to treat tapeworm infection, niclosamide has been often repurposed in treating

88   a wide range of diseases including several cancers, bacterial infections, viral infections, type 2

89   diabetes, non-alcoholic fatty liver disease, and rheumatoid arthritis[21]. This range of potential uses

90   is due to the significant polypharmacology of niclosamide, which is known to act on many

91   different biological targets and is a modulator of the Wnt/b-catenin, mTOR and JAK/STAT3

92   signaling pathways among others[21]. Niclosamide is also a weakly acidic lipophilic protonophore

93   that can disrupt pH gradients by shuttling protons across lipid membranes[22] including

94   mitochondria and lysosomes/endosomes. This physiochemical property is responsible for its

95   activity as a mitochondrial uncoupler[23] and contributes to its broad activity against viruses, many

96   of which rely on endosomal-cytoplasmic pH gradients in their life cycle[24].

4

97   Niclosamide was also previously identified as a potential antiviral for the related coronavirus

98   SARS-CoV, where it was shown to inhibit viral replication *in vitro* with low micromolar

99   potency[25]. The mechanism of action (MOA) for niclosamide against SARS-CoV-2 may be more

100   complex and multimodal than for SARS-CoV. Niclosamide has been shown to inhibit SARS-

101   CoV-2 endocytosis mediated entry[26], block viral replication by promoting cellular autophagy[27],

102   and disrupt spike (S) protein-mediated syncytia formation via inhibition of the host cell calcium-

103   dependent scramblase TMEM16F[28]. Given the polypharmacology of niclosamide, it is likely that

104   there are additional factors that contribute to its overall efficacy and complicate its MOA. The

105   degree to which each of these MOAs plays a role in the antiviral efficacy of niclosamide against

106   SARS-CoV-2 is unclear.

107   While niclosamide was clinically effective as an anthelmintic drug, it has substantial limitations

108   for use as a COVID-19 antiviral including its low oral bioavailability (<10%) and poor water

109   solubility[29,30]. Oral administration of niclosamide at 5 mg/kg in rats reaches a maximal serum

110   concentration (C_{max}) of only 354 ± 152 ng/mL[31]. As a result, the concentration of niclosamide in

111   the lungs would likely be too low to achieve therapeutic effect. Another limitation exists in that

112   polypharmacology is generally associated with increased adverse effects for repurposed drugs[32].

113   Finally, the toxicity of niclosamide is a major concern as it has been previously repurposed as a

114   broad anti-cancer agent and has shown significant cytotoxic/cytostatic effects *in vitro*[33,34]. A

115   better understanding of the anti-SARS-CoV-2 mechanism of action for niclosamide, including

116   potential toxicity and activity against emerging variants of concern (VOC), is needed to

117   effectively evaluate its clinical potential.

118   The goal of this study was to expand upon the understanding of niclosamide anti-SARS-CoV-2

119   activity and its potential as a clinical therapeutic using high content fluorescence imaging and

5

120   analysis. Herein, we reveal some of the mechanistic and cell morphological characteristics of

121   niclosamide activity, including an analysis of its cellular toxicity after long-term exposure to a

122   therapeutic antiviral dose. Additionally, we investigate niclosamide antiviral activity against

123   SARS-CoV-2 viral VOCs. We hypothesized that because the fusogenicity amongst SARS-CoV-

124   2 variants is known to be different[35–37], the potency/efficacy of niclosamide may also vary

125   between strains. Here we reveal the potency of niclosamide against several variants including

126   WA1 (wildtype), B.1.1.7 (alpha), B.1.351 (beta), P.1 (gamma) and B.1.617.2 (delta). Lastly, we

127   report the *in vitro* results of a structure-activity relationship (SAR) campaign of 33 niclosamide

128   analogs against SARS-CoV-2 in two different cell lines (VeroE6 and H1437). We used the

129   results from this SAR campaign to reveal additional mechanistic details for niclosamide, and aid

130   with the identification of structural analogs with reduced cellular toxicity. Altogether, our results

131   suggest that niclosamide itself is not a suitable candidate for the treatment of COVID-19, yet

132   there is potential for developing analogs with improved properties for future clinical use.

133   **Results**

134   **Niclosamide has a poor selectivity index**

135   One major concern regarding the utility of niclosamide as a COVID-19 antiviral is its

136   cytotoxicity in comparison with its antiviral efficacy. Here, we aimed to determine the selectivity

137   index (SI) of niclosamide *in vitro* against SARS-CoV-2 in two different cell models for

138   infection, VeroE6 and the human lung adenocarcinoma cell line H1437. To assess compound-

139   related toxicity, we evaluated the effects of niclosamide on cells after 72 hours of compound

140   exposure. We designed and optimized two separate high-content fluorescence imaging assays in

141   384-well plate format using the different cell lines and measured cell viability and viral

142   inhibition concurrently. In both assays, we used the detection of viral nucleocapsid (N) protein as

143   a direct marker for SARS-CoV-2 infection and cell count per well as an indicator of cell

144   viability. As summarized in the **Figure 1A** workflow, VeroE6 or H1437 cells were preincubated

145   with a 10-point 2-fold dilution series of niclosamide (N=10 replicates per condition) for 24 hours

146   and then infected with the SARS-CoV-2 B.1.1.7 variant for an additional 48 hours post-infection

147   (p.i.). Following infection, cells were fixed, permeabilized, and stained to identify nuclei and

148   viral N protein. Assay plates were imaged at 10X magnification using a CX5 high content

149   imaging platform (N=9 fields captured per well) and processed using the image segmentation

150   and analysis software CellProfiler. Data from the CellProfiler output were used to determine

151   percent infection and percent viability. Infection data were normalized to the average well-level

152   % N positive for infected controls (mock) in each cell line (**Supplementary Figure S1A**).

153   Percent viability was determined by normalizing the average well-level cell counts for the

154   infected control (**Supplementary Figure S1B**). We found that niclosamide has potent 50%

155   maximal inhibition (IC_{50}) values of 564 nM for VeroE6 and 261 nM for H1437. However,

156   niclosamide caused a 50% reduction in cell viability (CC_{50}) at concentrations of 1050 nM and

157   438 nM for VeroE6 and H1437, respectively, resulting in poor selectivity indices in both cell

158   lines (1.86 for VeroE6 and 1.67 for H1437). The concentration-response curves for this

159   experiment are shown in **Figure 1B** along with representative images for infected control, mock,

160   and 10 μM niclosamide conditions for each cell line. As illustrated in **Figure 2B** and

161   Supplementary **Figure 1A**, the average percentage of N protein-positive cells in untreated

162   infected controls after 48 hours of infection was significantly higher in VeroE6 (69 %) than

163   H1437 (9%) indicating more efficient cell-to-cell spread in the former. In conclusion,

164   niclosamide has a low SI in two cell lines of fibroblast origin, representing a liability for

165   therapeutic use.

Niclosamide potency is SARS-CoV-2 variant dependent

Niclosamide has a complex polypharmacology profile against host-cell pathways, which may contribute to the antiviral efficacy and/or cytotoxicity of the compound and lead to variable responses across SARS-CoV-2 VOCs that rely differentially on these pathways. To evaluate the antiviral efficacy of niclosamide against VOCs, we used a modified infection assay in VeroE6. Exposure to niclosamide was reduced to a 1- hour preincubation and the assay window was shortened to 24 hours post-infection (**Figure 2A**) to limit compound toxicity. VeroE6 cells were used as they demonstrated a higher N-protein positivity rate than H1437 cells. We evaluated the antiviral activity of niclosamide against the WA1 (wildtype), B.1.1.7 (alpha), B.1.351 (beta), P.1 (gamma), and B.1.617.2 (delta) variants in 10-point, 2-fold dilution. 10-Point dose-response efficacy experiments showed niclosamide had statistically significant differences in efficacy against VOCs, was most potent against the B.1.1.7 strain (IC_{50} = 298 nM), and least potent against the WA1 strain (IC_{50} = 1664 nM). The full efficacy data for all variants are shown in **Figures 2B-C**. The CC_{50} for niclosamide in this shortened assay was > 10 μM (not shown). These data demonstrate variant dependent antiviral efficacy of niclosamide.

High-content analysis suggests inhibition of entry and syncytia formation

Cell morphologic analysis of cells infected with VOCs, under the treatment of niclosamide, revealed several defining characteristics of infection influenced by compound treatment. We quantified these observations using morphological cell profiling analysis. We used data (B.1.1.7 variant in VeroE6) from the viral control (mock) and three different efficacious concentrations of niclosamide around its IC_{50} (156 nM, 313 nM, 625 nM) to reanalyze using a more extensive analysis pipeline that included intensity and area/shape measurements for both nuclear and viral

8

188   channels. For this analysis, syncytia/individually infected cells were defined as "viral objects."

189   We determined that treatment with niclosamide decreased the maximum size of syncytia (**Figure**

190   **3A**) consistent with an inhibition of cell-to-cell spread. We also found that treatment reduced the

191   number of individually infected cells within a well (**Figure 3B**) consistent with an inhibition of

192   viral entry. Finally, we found that the N protein intensity of remaining viral objects increased

193   with escalating concentrations of niclosamide (**Figure 3C**). The combination of these

194   observations suggests multiple MOA including inhibition of viral entry and cell-to-cell spread

195   resulting in fewer infected cells with dramatically increased cellular viral N protein content.

196   These results provide support for the polypharmacology of niclosamide that contributes to

197   multimodal efficacy against SARS-CoV-2. In addition, these results suggest that niclosamide

198   may not directly inhibit viral replication *in vitro*.

199   **Structure-activity relationship of niclosamide analogs versus SARS-CoV-2 infection**

200   Efficacy and cytotoxicity of 33 previously designed analogs[38] of niclosamide were used to

201   establish a preliminary structure-activity relationship (SAR) profile for niclosamide for anti-

202   SARS-CoV-2 activity in VeroE6 and H1437 cell lines. These analogs were also salicylanilides

203   and had substituent modifications on the nitroaniline and/or chlorosalicyl rings (**Figure 4A**)

204   intending to improve the selectivity while maintaining antiviral efficacy. Analog structures are

205   shown in **Supplementary Figure S2**. Analogs were evaluated using the assay described in

206   **Figure 1A**. All analogs were tested in 10-point 2-fold dilution series (N=3) from a starting

207   concentration of 20 μM. VeroE6 analog screening was performed using the B.1.1.7 variant at an

208   MOI of 0.1, while H1437 screening was performed using the WA1 variant at an MOI of 1. The

209   results from compound testing are summarized in **Table 1**, which includes IC_{50} and CC_{50} values

210   for both cell lines. As shown in Table 1, we found that 14 analogs retained IC_{50} values in the

211   nanomolar or micromolar range in VeroE6, while seven (compounds 2, 3, 4, 11, 12, 24, 34) were

212   efficacious in both VeroE6 and H1437. Four compounds (2, 7, 11, 24) showed improved potency

213   and reduced cytotoxicity against VeroE6 compared to niclosamide (**Figure 4C-F**). Overall,

214   improvements in cytotoxicity were less pronounced against H1437. Notably, the variant

215   dependent potency difference was conserved in H1437 cells and was significantly less potent

216   against WA1 (IC_{50} = 16770 nM) than B.1.1.7 (IC_{50} = 261 nM), consistent with results in VeroE6

217   cells.

218   In general, we found that the replacement of the nitro group on the nitroaniline ring was well

219   tolerated (compounds 5, 6, 7, 10, 24 and 34) and improved the selectivity index. We also noted

220   that modification to the chloro position on the salicylic acid ring (R2) was well tolerated and all

221   compounds with only this modification retained antiviral efficacy (compounds 2, 3, 4, 11, 12).

222   Many analogs (compounds 7,8, 10, 14-19, 22, 25, 28-30, and 33) were found to exacerbate

223   infection in H1437 cells (**Supplementary Figure S3**) and showed inverted concentration-

224   response curves at high concentrations. Remarkably, the removal of the hydroxyl group (R1) on

225   the salicylic acid ring (compound 9) resulted in a complete loss of activity in both VeroE6 and

226   H1437 (**Figure 5A**). This hydroxyl group has been previously reported as the protonophore

227   responsible for the mitochondrial uncoupling activity of niclosamide[23,38].

228   Given the drastic loss of activity, we evaluated the anti-SARS-CoV-2 efficacy of other

229   protonophore mitochondrial uncouplers including FCCP[39], 2,4 DNP[40], oxyclozanide[41] and

230   dicumarol[42]. These compounds were evaluated against WA1 and B.1.1.7 variants in VeroE6 cells

231   using the 24-hour infection conditions described in **Figure 3A**. Both FCCP and oxyclozanide

232   showed efficacy in the micromolar range (**Figure 5B-F**). The potency of these compounds was

233   higher against B.1.1.7 than WA1, however the difference was more pronounced for niclosamide.

10

234   These results indicate that the mechanism of action for niclosamide against SARS-CoV-2 is at

235   least partially due to its physiochemical property as a protonophore, implicating energetic stress

236   response pathways in SARS-CoV-2 infection.

Discussion

238   There remains an urgent need for COVID-19 therapeutics, which can be used to prevent or treat

239   the spread of the virus SARS-CoV-2. The FDA approved oral anthelmintic drug niclosamide has

240   antiviral activity against SARS-CoV-2 infection *in vitro* and *in* vivo[43], which has generated

241   interest in its application for the treatment of COVID-19 and resulted in the conductance of

242   several human clinical trials. However, given its high cytotoxicity, unknown efficacy against

243   SARS-CoV-2 variants, low systemic bioavailability, and significant polypharmacology, we were

244   hesitant to consider niclosamide as a promising antiviral option. In this study, we used high-

245   content imaging of SARS-CoV-2 infected cells to evaluate some of the limitations of

246   niclosamide as a COVID-19 antiviral. We also extended our studies to structural analogs of

247   niclosamide, intending to reveal a preliminary structure-activity relationship profile that could be

248   used for future compound development.

249   Niclosamide has potent cytotoxic/cytostatic effects when applied directly to cells *in vitro*[34],

250   suggesting that it may have high acute toxicity *in vivo* with increased systemic exposure.

251   Clinically, the cytotoxicity is limited by the poor bioavailability of niclosamide, which has low

252   systemic exposure. To evaluate niclosamide toxicity, we used high-content fluorescence imaging

253   to determine a selectivity index for niclosamide in two different cell models including VeroE6

254   and the more physiologically relevant human lung adenocarcinoma cell line H1437. We found

255   that niclosamide has a very poor selectivity index in both cell lines (SI <2) after 72 hours of

256   compound exposure, suggesting that it would likely have a small therapeutic window clinically

11

257   even if the compound exposure was high enough in the lungs for antiviral efficacy. Longer

258   durations of exposure to niclosamide at relevant antiviral concentrations are likely to cause

259   significant side effects, which limits clinical application. Further studies are needed to evaluate

260   the safety of niclosamide at antiviral concentrations *in vivo*.

261   Our results are consistent with the results from recent clinical studies of niclosamide. Since it

262   was identified as an anti-SARS-CoV-2 agent *in vitro*, there have been several clinical studies to

263   evaluate the antiviral efficacy and safety of niclosamide. Notably, a recent phase 2 clinical trial

264   using 2g of orally administered niclosamide for 7 days revealed no statistically significant effect

265   on the duration of the contagious period of SARS-CoV-2[44]. While niclosamide was well

266   tolerated in this trial, the low efficacy and low adverse event rate are likely because the systemic

267   exposure is lower than what is required to observe antiviral activity or compound-related

268   toxicity. To address the poor oral bioavailability, several different formulations have been

269   developed for niclosamide to improve its exposure to the necessary site of action[45,46]. This has

270   included a formulation as an inhalable/intranasal powder to increase compound exposure in the

271   lungs. Unfortunately, a recent phase-1 safety trial using 50 mg over 2.5 days of

272   inhalable/intranasal niclosamide revealed moderate lung irritation in 59% of participants, which

273   suggests compound-related toxicity may be playing a significant role at higher local

274   concentrations in the lungs[47]. Although niclosamide is generally well-tolerated when used as an

275   anthelmintic drug, this is because it has low bioavailability, poor solubility, and stays within the

276   GI tract with very low systemic exposure.

277   A further limitation for using niclosamide as a COVID-19 therapeutic is its unknown efficacy

278   against the different emerging SARS-CoV-2 VOCs. We determined the efficacy for niclosamide

279   against the WA1 (wildtype), B.1.1.7 (alpha), B.1.351 (beta), P.1 (gamma) and B.1.617.2 (delta)

280   variants in VeroE6 cells. We found that there were significant differences in potency ranging

281   from 298 nM (beta variant) to 1664 nM (wildtype). Interestingly, the trend in potency correlates

282   with the ACE2 binding affinity for the different variants[48]. Variants, including alpha and beta,

283   also have higher fusogenicity than the wildtype variant and are more likely to undergo cell-to-

284   cell spread by syncytia[35], which may help explain the differences in potency.

285   These results are in contrast with those reported by Weiss *et al.*, which showed no significant

286   difference in potency amongst variants[49]. However, their study used qRT-PCR of viral RNA to

287   determine IC_{50} values, which is far less sensitive than a high-content imaging approach and does

288   not provide information on the clinically relevant endpoint of cell-to-cell spread inhibition.

289   Given the differences in potency amongst SARS-CoV-2 variants of concern, there arises a

290   concern for the rapid development or selection of resistant strains that do not respond to

291   niclosamide treatment. While the emergence of drug resistance is possible for any mechanism of

292   action inhibiting SARS-CoV-2, the pronounced difference between niclosamide's efficacy

293   amongst the VOCs makes niclosamide resistance inexorable. Further studies to understand the

294   mechanistic differences underlying variant-dependent responses to drugs like niclosamide may

295   ultimately inform *de novo* drug development for COVID-19.

296   To understand the MOA, we used morphological profiling of B.1.1.7 infected VeroE6 cells to

297   evaluate the effect of niclosamide treatment on SARS-CoV-2 infection. We found that

298   niclosamide inhibits the spread of virus to adjacent cells in a concentration-dependent fashion as

299   indicated by the reduction in size of viral syncytia. We also observed that the total number of

300   viral objects (individually infected cells or syncytia) decreased with niclosamide treatment,

301   which is consistent with entry inhibition. For example, if niclosamide were only influencing cell-

302   to-cell spread, the total number of viral objects would remain constant and only the size of the

13

303   syncytia would be affected. While the complete mechanism of action for niclosamide is

304   complex, our results suggest that both inhibition of cell-to-cell spread and entry inhibition play a

305   role in its activity (**Figure 6**). The degree to which each of the MOAs contributes to efficacy may

306   be different for SARS-CoV-2 variants, which could help explain the differences in potency.

307   The polypharmacology of niclosamide is a major issue for its utility as a COVID-19 antiviral.

308   Niclosamide is known to influence many different signal transduction pathways and has been

309   implicated in the treatment of a wide range of diseases including several cancers, bacterial

310   infections, viral infections, type 2 diabetes, non-alcoholic fatty liver disease, rheumatoid arthritis,

311   and others. Unfortunately, the mechanism of action for niclosamide remains elusive for the

312   majority of its biological effects. It is often unclear if there is a direct interaction between

313   niclosamide and a molecular target, or if there is an indirect mechanism of action at play[21]. An

314   underlying mechanism for its broad activity may be its ability to act as a protonophore, which

315   has many different downstream effects in cells including disruption of pH gradients,

316   mitochondrial uncoupling, and transcriptional modulation of various gene targets[21]. This

317   mechanistic ambiguity also translates to its antiviral efficacy. It is likely that the antiviral

318   activities of niclosamide (e.g., inhibition of entry, replication, and syncytia formation) are all

319   downstream consequences of its activity as a nonspecific protonophore since activity was lost

320   following removal of the hydroxyl group. If this is the case, then it may be challenging to

321   separate the undesired off-target effects from the antiviral effects. While our studies suggest that

322   niclosamide and other mitochondrial uncouplers demonstrate anti-SARS-CoV-2 efficacy, further

323   studies are warranted to determine if these mechanisms of action are unified by protonophore

324   activity.

14

325   While niclosamide is not an ideal candidate itself, it may represent a promising chemical tool for

326   the development of more specific SARS-CoV-2 inhibitors. In particular, inhibition of cell-to-cell

327   spread by syncytia is an extremely attractive mechanism for inhibition. Syncytia, which are

328   multinucleated bodies resulting from the fusion of adjacent cells, are a key characteristic of

329   SARS-CoV-2 infection and have been observed in many post-mortem histological samples from

330   fatal COVID-19 cases[28,50]. Syncytia formation facilitates the rapid spread of the viral genome

331   between cells[51], which increases the area of infected tissue and may enhance immune system

332   evasion[52]. An inhibitor of cell-to-cell infection like niclosamide may be clinically useful for the

333   treatment or prevention of COVID-19, especially when cocktailed with other direct acting

334   antivirals.

335   In this study, we also tested the antiviral efficacy of 33 structural analogs of niclosamide to

336   establish a preliminary structure-activity relationship profile which could aid in the development

337   of compounds with antiviral efficacy and less off-target effects. We identified seven compounds

338   (compounds 2, 3, 4, 11, 12, 24, 34) that were efficacious in both VeroE6 and H1437 cell models

339   and four of which had improved potency and reduced cytotoxicity in VeroE6 (Compounds

340   2,7,11 and 24). Consequently, we believe there is a potential for designing better niclosamide

341   analogs with improved properties. Additionally, our structure-activity analysis revealed some

342   mechanistic features of niclosamide. Most noteworthy, the removal of the protonophore

343   hydroxyl group resulted in complete loss of activity in both cell models. The efficacy of analogs

344   strongly relied on their weakly acidic and lipophilic nature. Analogs with higher predicted

345   acidity (pKa) due to the presence of carboxylic acid substituents were generally completely

346   inactive. We also determined that other protonophores, including FCCP and oxyclozanide, also

347   had anti-SARS-CoV-2 efficacy, suggesting that the ability to disrupt pH gradients is central to

348   the mechanism of action for niclosamide. Niclosamide has been shown to neutralize endo-

349   lysosomal pH gradients, which is believed to be responsible for its broad-spectrum antiviral

350   activity[24]. Our results indicate that this nonspecific mechanism of action also significantly

351   contributes to the activity of niclosamide against SARS-CoV-2.

352   Overall, the poor selectivity index, low bioavailability, complex polypharmacology, nonspecific

353   protonophore activity, and variant-dependent potency of niclosamide limit its potential as a

354   COVID-19 therapeutic. However, our studies have shown that changes to the salicyl and aniline

355   rings can modulate selectivity and bioavailability while maintaining its activity. Therefore,

356   niclosamide represents a useful chemical probe that can be leveraged in a large-scale SAR

357   campaign to design better analogs in the future.

358   **Methods**

359   **Compounds**

360   Niclosamide, FCCP, 2,4 DNP, Oxyclozanide and Dicumarol were obtained from Sigma Aldrich

361   and prepared as 10 mM stock solutions in dimethylsulfoxide (DMSO). The 33 structural analogs

362   of niclosamide were obtained from previous studies[38]. Compounds were solubilized at 10 mM in

363   DMSO, and were dispensed onto cells using an HPD300e digital compound dispenser.

364   **Cells and Virus**

365   VeroE6 cells were maintained in Dulbecco's Modified Eagle Medium (DMEM), and H1437 cells

366   were maintained in RPMI 1640 base medium. Both cell lines were supplemented with 10% fetal

367   bovine serum (FBS) and 1X pen-strep solution and were grown at 37°C with 5% CO_2 following

368   standard cell culture procedures. These cell lines were tested for mycoplasma contamination

369   before use and were negative. The following reagents were deposited by the Centers for Disease

370   Control and Prevention and were obtained through BEI resources, NIAID, NIH: SARS-Related

371   Coronavirus 2, Isolate USA-WA1/2020, NR-52281, USA/CA_CDC_5574/2020 (B.1.1.7), NR-

372   54011, USA/MD-HP01542/2021 (Lineage B.1.351), NR-55282, Japan/TY7-503/2021 (Brazil

373   P.1), NR-54982, USA/PHC658/2021 (Lineage B.1.617.2), NR-55611.Viral stocks were grown in

374   VeroE6 and titers were determined by TCID50 using the Reed and Muench method[53]. All the

375   work with live SARS-CoV-2 virus was performed in biosafety level-3 containment lab (BSL3)

376   with the approval of the University of Michigan's Department of Environment and Health and

377   Safety and the Institutional Biosafety Committee.

378   **Anti-SARS-CoV-2 high content bioassays**

379   Assays were adapted from previous work and optimized for H1437 and VeroE6 cell lines[17,54].

380   For 48-hour infection experiments, VeroE6 and H1437 cells were seeded onto 384 well plates

381   (6057300, Perkin Elmer) at densities of 3000 and 5000 cells per well, respectively, in 50 µL of

382   media. After 24 hours of cell attachment at 37°C and 5% CO_2, compounds were dispensed

383   directly to the cell plates using an HPD300e digital compound dispenser. All wells were

384   normalized to a constant DMSO concentration of 0.2%, and plates contained both infected and

385   uninfected control wells. After 24 hours of preincubation with compounds, cells were inoculated

386   with the indicated SARS-CoV-2 variant at MOIs of 0.1 for VeroE6 and 1 for H1437. Cells were

387   incubated with virus and compounds for an additional 48 hours and then fixed with 4%

388   paraformaldehyde for 30 minutes at room temperature. Cells were then permeabilized with 0.3%

389   Triton-X100 for 15 minutes and stained with anti-nucleocapsid protein primary antibody

390   (ABIN6952432, Antibodies Online) at a dilution of 1:2000 overnight at +4°C. Following

391   primary antibody staining, cells were stained with a dye cocktail containing 1:1000 secondary

392   antibody Alexa-647 (goat anti-mouse, A21235, Thermo Fisher) and 10 µg/mL Hoechst 33342

393   pentahydrate (bis-benzimide) for nuclear labeling for a total of 30 minutes at room temperature.

394   Cells were stored in PBS before imaging. For 24-hour infection experiments, the methods were

395   comparable except that VeroE6 cells were seeded at 5000 cells per well, compounds were

396   preincubated for 1 hour instead of 24, and the infection window was 24 hours instead of 48. All

397   other inoculation, fixation and staining procedures were identical.

398   **High Content Imaging**

399   Stained assay plates were imaged using a both a Thermo Fisher CX5 with a 10X/0.45NA

400   objective lens and a Yokogawa Cell Voyager 8000 (CV8000) microscope with a 20X/1.0NA

401   water immersion lens. Imaging techniques were followed as described previously for detection

402   of nuclei and SARS-CoV-2 nucleocapsid protein[17,54]. A total of N=9 fields per well were imaged

403   for all assay plates, accounting for roughly 80% of the total well area.

404   **Image Processing**

405   Images were processed using the image segmentation and analysis software CellProfiler 4.0[55].

406   Separate pipelines were developed for H1437 and VeroE6 images. Pipelines were used to

407   identify nuclei (Hoechst 33342) and viral objects including multinucleated syncytia and

408   individually infected cells (Alexa Fluor 647) by adaptive otsu thresholding. Similar to previous

409   work, infected cells were identified using the *relateobjects* module whereby any nucleus

410   contained within a viral object was defined as infected[54]. For morphological profiling of B.1.1.7

411   infection vs. niclosamide in VeroE6, additional intensity, textural and spatial features were

412   measured using CellProfiler 4.0 for both the nuclear and viral channels.

413

414

Concentration response analysis and IC_{50}/CC_{50} determination

Field level data were grouped at the well level using Knime[56] and used to determine normalized

percent infection and percent viability scores. Raw percent infection per well was determined by

taking the ratio of infected nuclei to total nuclei and multiplying by 100. Normalized percent

infection was then generated such that "100% infection" was equivalent to the average raw

percent infection of the viral control for each plate. Cell counts for the entire plate were

normalized and 100% viability was based on the average cell count of the infected DMSO

control wells. Concentration-response curves were plotted in GraphPad Prism 9.0 (GraphPad

Software) and fitted using a semi-log 4-parameter variable slope model. IC_{50} and CC_{50} values were

extracted from percent infection curves and percent viability curves, respectively. Selectivity

indices were determined by taking a ratio of the CC_{50} and IC_{50}.

High content imaging analysis of B.1.1.7 infection versus niclosamide

Object level data for nuclei and viral objects (syncytia and individually infected cells) was used

to evaluate morphological and phenotypic features of B.1.1.7 infection versus niclosamide

including changes in N protein intensity and area of viral objects. Only images for the infected

DMSO vehicle control, as well as 3 different concentrations of niclosamide (156 nM, 313 nM

and 625 nM) were included in this analysis. The max viral object area reported in Figure 3A

represents the largest viral object observed for each condition including all fields and replicate

wells. The mean N protein intensity for infected cells was computed at the object level and the

results from Figure 3C include data for cells in each condition.

19

438

Statistical analysis and hypothesis testing

All statistical analyses and hypothesis testing was performed using GraphPad Prism 9.0

(GraphPad software). Specifics for statistical analyses, including sample sizes and other

important data are included within the text of figure legends.

Acknowledgements

References

1. Hu, B., Guo, H., Zhou, P. & Shi, Z. L. Characteristics of SARS-CoV-2 and COVID-19. *Nature Reviews Microbiology 2020 19:3* **19**, 141–154 (2020).

2. Aslan, A., Aslan, C., Zolbanin, N. M. & Jafari, R. Acute respiratory distress syndrome in COVID-19: possible mechanisms and therapeutic management. *Pneumonia 2021 13:1* **13**, 1–15 (2021).

3. Mizrahi, B. *et al.* Longitudinal symptom dynamics of COVID-19 infection. *Nature Communications 2020 11:1* **11**, 1–10 (2020).

4. Dong, E., Du, H. & Gardner, L. An interactive web-based dashboard to track COVID-19 in real time. *Lancet Infect Dis* **20**, 533–534 (2020).

5. Harvey, W. T. *et al.* SARS-CoV-2 variants, spike mutations and immune escape. *Nat Rev Microbiol* **19**, 409–424 (2021).

465   6.   Kyriakidis, N. C., López-Cortés, A., González, E. V., Grimaldos, A. B. & Prado, E. O. SARS-CoV-2
466   vaccines strategies: a comprehensive review of phase 3 candidates. *npj Vaccines 2021 6:1* **6**, 1–17
467   (2021).

468   7.   Cully, M. A tale of two antiviral targets - and the COVID-19 drugs that bind them. *Nat Rev Drug
469   Discov* **21**, 3–5 (2022).

470   8.   Whitley, R. Molnupiravir — A Step toward Orally Bioavailable Therapies for Covid-19. *New
471   England Journal of Medicine* **386**, 592–593 (2022).

472   9.   Hammond, J. *et al.* Oral Nirmatrelvir for High-Risk, Nonhospitalized Adults with Covid-19. *New
473   England Journal of Medicine* **386**, 1397–1408 (2022).

474   10.   Feinmann, J. Covid-19: global vaccine production is a mess and shortages are down to more than
475   just hoarding. *BMJ* **375**, (2021).

476   11.   Qomara, W. F., Primanissa, D. N., Amalia, S. H., Purwadi, F. v. & Zakiyah, N. Effectiveness of
477   Remdesivir, Lopinavir/Ritonavir, and Favipiravir for COVID-19 Treatment: A Systematic Review.
478   *Int J Gen Med* **14**, 8557–8571 (2021).

479   12.   Gottlieb, R. L. *et al.* Early Remdesivir to Prevent Progression to Severe Covid-19 in Outpatients. *N
480   Engl J Med* **386**, 305–315 (2022).

481   13.   Chen, R. E. *et al.* Resistance of SARS-CoV-2 variants to neutralization by monoclonal and serum-
482   derived polyclonal antibodies. *Nature Medicine 2021 27:4* **27**, 717–726 (2021).

483   14.   Takashita, E. *et al.* Efficacy of Antiviral Agents against the SARS-CoV-2 Omicron Subvariant BA.2.
484   *New England Journal of Medicine* **386**, 1475–1477 (2022).

485   15.   Pushpakom, S. *et al.* Drug repurposing: progress, challenges and recommendations. *Nature
486   Reviews Drug Discovery 2018 18:1* **18**, 41–58 (2018).

487   16.   Drayman, N. *et al.* Masitinib is a broad coronavirus 3CL inhibitor that blocks replication of SARS-
488   CoV-2. *Science (1979)* **373**, 931–936 (2021).

489   17.   Mirabelli, C. *et al.* Morphological cell profiling of SARS-CoV-2 infection identifies drug repurposing
490   candidates for COVID-19. *Proc Natl Acad Sci U S A* **118**, (2021).

491   18.   Touret, F. *et al.* In vitro screening of a FDA approved chemical library reveals potential inhibitors
492   of SARS-CoV-2 replication. *Scientific Reports* **10**, 13093 (2020).

493   19.   Xiao, X. *et al.* Identification of Potent and Safe Antiviral Therapeutic Candidates Against SARS-
494   CoV-2. *Frontiers in Immunology* **11**, (2020).

495   20.   Jeon, S. *et al.* Identification of antiviral drug candidates against SARS-CoV-2 from FDA-approved
496   drugs. *Antimicrobial Agents and Chemotherapy* **64**, (2020).

497   21.   Chen, W., Mook, R. A., Premont, R. T. & Wang, J. Niclosamide: Beyond an antihelminthic drug.
498   *Cellular Signalling* **41**, 89–96 (2018).

499   22.   Fonseca, B. D. *et al.* Structure-activity analysis of niclosamide reveals potential role for
500   cytoplasmic pH in control of mammalian target of rapamycin complex 1 (mTORC1) signaling. *J*
501   *Biol Chem* **287**, 17530–17545 (2012).

502   23.   Kumar, R. *et al.* Mitochondrial uncoupling reveals a novel therapeutic opportunity for p53-
503   defective cancers. *Nature Communications 2018 9:1* **9**, 1–13 (2018).

504   24.   Jurgeit, A. *et al.* Niclosamide Is a Proton Carrier and Targets Acidic Endosomes with Broad
505   Antiviral Effects. *PLoS Pathogens* **8**, 1002976 (2012).

506   25.   Wu, C. J. *et al.* Inhibition of Severe Acute Respiratory Syndrome Coronavirus Replication by
507   Niclosamide. *Antimicrobial Agents and Chemotherapy* **48**, 2693 (2004).

508   26.   Prabhakara, C. *et al.* Strategies to target SARS-CoV-2 entry and infection using dual mechanisms
509   of inhibition by acidification inhibitors. *PLOS Pathogens* **17**, e1009706 (2021).

510   27.   Gassen, N. C. *et al.* SARS-CoV-2-mediated dysregulation of metabolism and autophagy uncovers
511   host-targeting antivirals. *Nature Communications 2021 12:1* **12**, 1–15 (2021).

512   28.   Braga, L. *et al.* Drugs that inhibit TMEM16 proteins block SARS-CoV-2 spike-induced syncytia.
513   *Nature 2021 594:7861* **594**, 88–93 (2021).

514   29.   Lin, C. K. *et al.* Preclinical evaluation of a nanoformulated antihelminthic, niclosamide, in ovarian
515   cancer. *Oncotarget* **7**, 8993 (2016).

516   30.   Fan, X., Li, H., Ding, X. & Zhang, Q. Y. Contributions of Hepatic and Intestinal Metabolism to the
517   Disposition of Niclosamide, a Repurposed Drug with Poor Bioavailability. *Drug Metab Dispos* **47**,
518   756–763 (2019).

519   31.   Chang, Y. W. *et al.* Pharmacokinetics of anti-SARS-CoV agent niclosamide and its analogs in rats.
520   *Journal of Food and Drug Analysis* **14**, 15 (2020).

521   32.   Reddy, A. S. & Zhang, S. Polypharmacology: drug discovery for the future. *Expert Rev Clin*
522   *Pharmacol* **6**, 41–47 (2013).

523   33.   Wieland, A. *et al.* Anticancer effects of niclosamide in human glioblastoma. *Clin Cancer Res* **19**,
524   4124–4136 (2013).

525   34.   Hamdoun, S., Jung, P. & Efferth, T. Drug repurposing of the anthelmintic niclosamide to treat
526   multidrug-resistant leukemia. *Frontiers in Pharmacology* **8**, (2017).

527   35.   Rajah, M. M. *et al.* SARS-CoV-2 Alpha, Beta, and Delta variants display enhanced Spike-mediated
528   syncytia formation. *EMBO J* **40**, (2021).

529   36.   Saito, A. *et al.* Enhanced fusogenicity and pathogenicity of SARS-CoV-2 Delta P681R mutation.
530   *Nature* **602**, 300–306 (2022).

531   37.   Zhang, Y. *et al.* SARS-CoV-2 spike L452R mutation increases Omicron variant fusogenicity and
532   infectivity as well as host glycolysis. *Signal Transduction and Targeted Therapy 2022 7:1* **7**, 1–3
533   (2022).

bioRxiv preprint doi: https://doi.org/10.1101/2022.06.24.497526; this version posted July 13, 2022. The copyright holder for this preprint (which was not certified by peer review) is the author/funder, who has granted bioRxiv a license to display the preprint in perpetuity. It is made available under aCC-BY-NC-ND 4.0 International license.

534 38. Bhagat, H. A. *et al.* N-substituted phenylbenzamides of the niclosamide chemotype attenuate
535   obesity related changes in high fat diet fed mice. *PLOS ONE* **13**, e0204605 (2018).

536 39. Park, K. S. *et al.* FCCP depolarizes plasma membrane potential by activating proton and Na+
537   currents in bovine aortic endothelial cells. *Pflugers Archiv : European journal of physiology* **443**,
538   344–352 (2002).

539 40. Blaikie, F. H. *et al.* Targeting dinitrophenol to mitochondria: limitations to the development of a
540   self-limiting mitochondrial protonophore. *Biosci Rep* **26**, 231–243 (2006).

541 41. Shrestha, R., Johnson, E. & Byrne, F. L. Exploring the therapeutic potential of mitochondrial
542   uncouplers in cancer. *Molecular Metabolism* **51**, 101222 (2021).

543 42. Kotova, E. A. & Antonenko, Y. N. Fifty Years of Research on Protonophores: Mitochondrial
544   Uncoupling As a Basis for Therapeutic Action. *Acta Naturae* **14**, 4 (2022).

545 43. Blake, S. *et al.* Salicylanilides Reduce SARS-CoV-2 Replication and Suppress Induction of
546   Inflammatory Cytokines in a Rodent Model. *ACS Infectious Diseases* **7**, 2229–2237 (2021).

547 44. Cairns, D. M. *et al.* Efficacy of Niclosamide vs Placebo in SARS-CoV-2 Respiratory Viral Clearance,
548   Viral Shedding, and Duration of Symptoms Among Patients With Mild to Moderate COVID-19: A
549   Phase 2 Randomized Clinical Trial. *JAMA Network Open* **5**, e2144942–e2144942 (2022).

550 45. Parikh, M. *et al.* Phase Ib trial of reformulated niclosamide with abiraterone/prednisone in men
551   with castration-resistant prostate cancer. *Scientific Reports 2021 11:1* **11**, 1–7 (2021).

552 46. Lin, C. K. *et al.* Preclinical evaluation of a nanoformulated antihelminthic, niclosamide, in ovarian
553   cancer. *Oncotarget* **7**, 8993 (2016).

554 47. Backer, V. *et al.* A randomized, double-blind, placebo-controlled phase 1 trial of inhaled and
555   intranasal niclosamide: A broad spectrum antiviral candidate for treatment of COVID-19. *The
556   Lancet Regional Health - Europe* **4**, 100084 (2021).

557 48. Liu, H., Wei, P., Kappler, J. W., Marrack, P. & Zhang, G. SARS-CoV-2 Variants of Concern and
558   Variants of Interest Receptor Binding Domain Mutations and Virus Infectivity. *Frontiers in
559   Immunology* **13**, 50 (2022).

560 49. Weiss, A. *et al.* Niclosamide shows strong antiviral activity in a human airway model of SARS-CoV-
561   2 infection and a conserved potency against the Alpha (B.1.1.7), Beta (B.1.351) and Delta variant
562   (B.1.617.2). *PLOS ONE* **16**, e0260958 (2021).

563 50. Bussani, R. *et al.* Persistence of viral RNA, pneumocyte syncytia and thrombosis are hallmarks of
564   advanced COVID-19 pathology. *EBioMedicine* **61**, (2020).

565 51. Lin, L., Li, Q., Wang, Y. & Shi, Y. Syncytia formation during SARS-CoV-2 lung infection: a disastrous
566   unity to eliminate lymphocytes. *Cell Death & Differentiation 2021 28:6* **28**, 2019–2021 (2021).

567 52. Rajah, M. M., Bernier, A., Buchrieser, J. & Schwartz, O. The Mechanism and Consequences of
568   SARS-CoV-2 Spike-Mediated Fusion and Syncytia Formation. *Journal of Molecular Biology* **434**,
569   167280 (2022).

570   53.   Reed, L. J. & Muench, H. A simple method of estimating fifty per cent endpoints. *American
571   Journal of Epidemiology* **27**, 493–497 (1938).

572   54.   Wotring, J. W., Fursmidt, R., Ward, L. & Sexton, J. Z. Evaluating the in vitro efficacy of bovine
573   lactoferrin products against SARS-CoV-2 variants of concern. *J Dairy Sci* **105**, 2791–2802 (2022).

574   55.   McQuin, C. *et al.* CellProfiler 3.0: Next-generation image processing for biology. *PLOS Biology* **16**,
575   e2005970 (2018).

576   56.   Berthold, M. R. *et al.* KNIME - the Konstanz information miner. *ACM SIGKDD Explorations
577   Newsletter* 58–61 (2009) doi:10.1145/1656274.1656280.

578

579

580

581

582

583

584

585

586

587

588

589

590

591

592

593

594

595

596

597

598

599

pageFigures

A.)

B.)
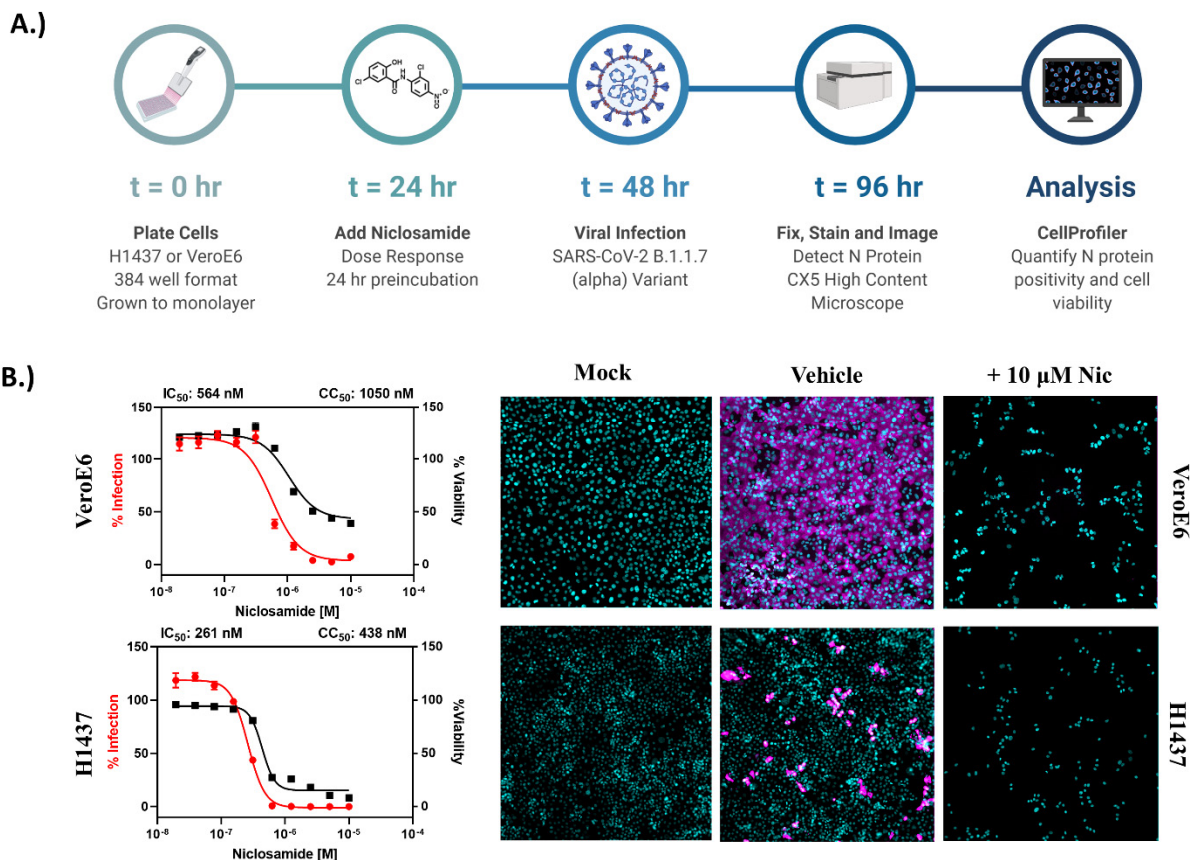
Figure 1. Niclosamide is toxic at antiviral concentrations after long term exposure. A.)

Workflow for high content anti-SARS-CoV-2 bioassay screening to determine infection

inhibition and cytotoxicity. B.) 10-point, 2-fold dilution concentration-response curves for

VeroE6 and H1437 cells with a starting concentration of 10 μM. VeroE6 cells were infected with

SARS-CoV-2 B.1.1.7 variant at a multiplicity of infection (MOI) of 0.1, while H1437 were

infected with SARS-CoV-2 WA1 variant at an MOI =1 to achieve optimal infection at 48 hours

post-infection. Data points represent mean ± SEM for N=10 replicates per condition. Curve

fitting was performed in GraphPad Prism 9.0 using a semi-log 4-parameter variable slope model.

Representative overlay images for mock, vehicle, and 10 μM Niclosamide treatment (infected)

are included (cyan = nuclei, magenta = SARS-CoV-2 N protein).

25
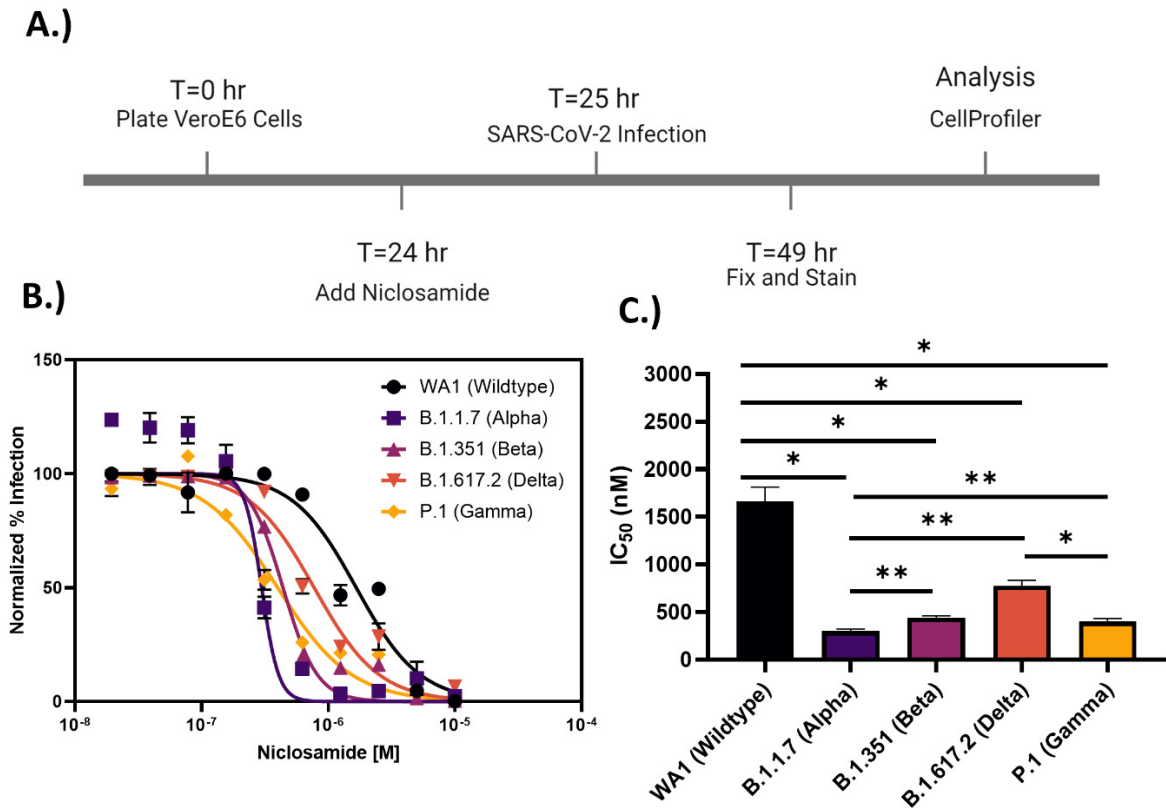
Figure 2. Niclosamide potency is SARS-CoV-2 variant dependent. A.) Assay timeline for 24-hour infection experiment. The assay window was shortened to reduce niclosamide toxicity. B.) 10-point 2-fold concentration-response curves for niclosamide against the different SARS-CoV-2 variants of concern (MOI = 0.1 for each variant) with a top concentration of 10μM. Curves were fitted with GraphPad Prism 9.0 software using a semi-log 4-parameter variable slope model. Data for each variant was normalized to the average percent infected of its respective viral control. Data points represent mean ± SEM for N=3 replicates. C.) IC_{50} values for niclosamide potency against SARS-CoV-2 variants of concern. Values were extracted from curve fitting using GraphPad 9.0 and include SEM error bars (WA1: 1664 ± 149 nM, B.1.1.7: 298 ± 23 nM, B.1.351: 440 ± 21 nM, B.1.617.2: 774 ± 58 nM, P.1: 399 ± 34 nM). Significance was determined using Student's T-tests (* = $P<0.05$, ** = $P<0.01$).

26
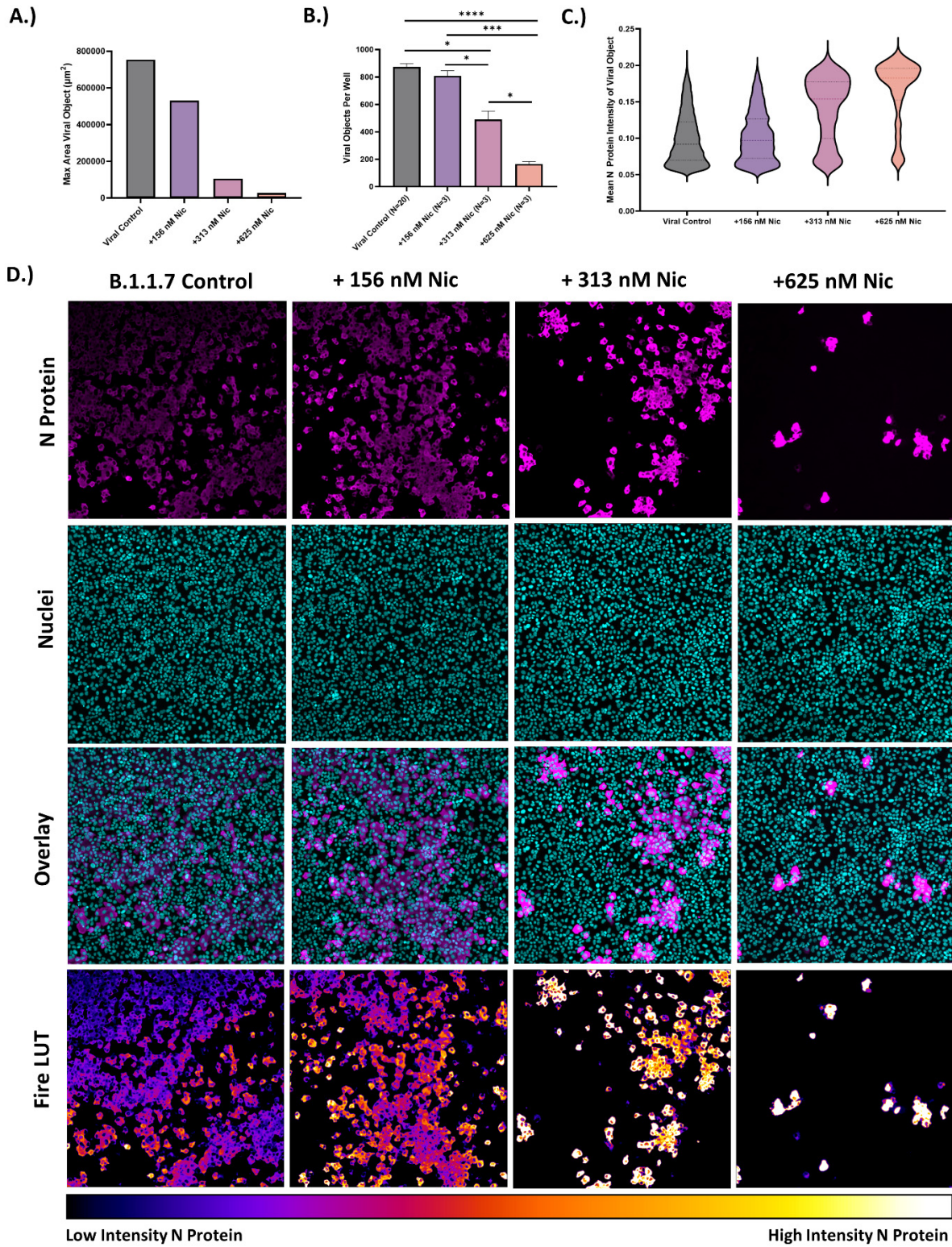
626 **Figure 3. Morphological profiling of B.1.1.7 infection versus niclosamide treatment in**

627 **VeroE6.** Image analysis reveals mechanistic characteristics of niclosamide activity against

628 SARS-CoV-2 infection. A.) The maximum area of viral objects decreases with increasing

629 niclosamide concentration. Data is the max area for viral objects in each condition. Viral control:

630 N=17452, +156 nM niclosamide: N=2425, +313 nM niclosamide: N= 1470, +625 nM

631 niclosamide: N= 496. B.) Viral objects per well decreases with increasing niclosamide

632 concentration. Viral objects include single infected cells and syncytia. Replicate values are

633 indicated on the X axis. C.) Mean pixel intensity for viral objects in each condition. Pixel

634 intensity increases with increasing niclosamide concentration. D.) Representative images for

635 each condition including N-protein channel, nuclear channel, an overlayed image and a fire

636 lookup table (LUT) image of the N-protein channel. Images were taken on a CX5 high content

637 microscope at 10X magnification. * = P<0.05, ***= P<0.001, ****= P<0.0001.

638

639

640

641

642

643

644

645

646

647

648

649

650

651

28
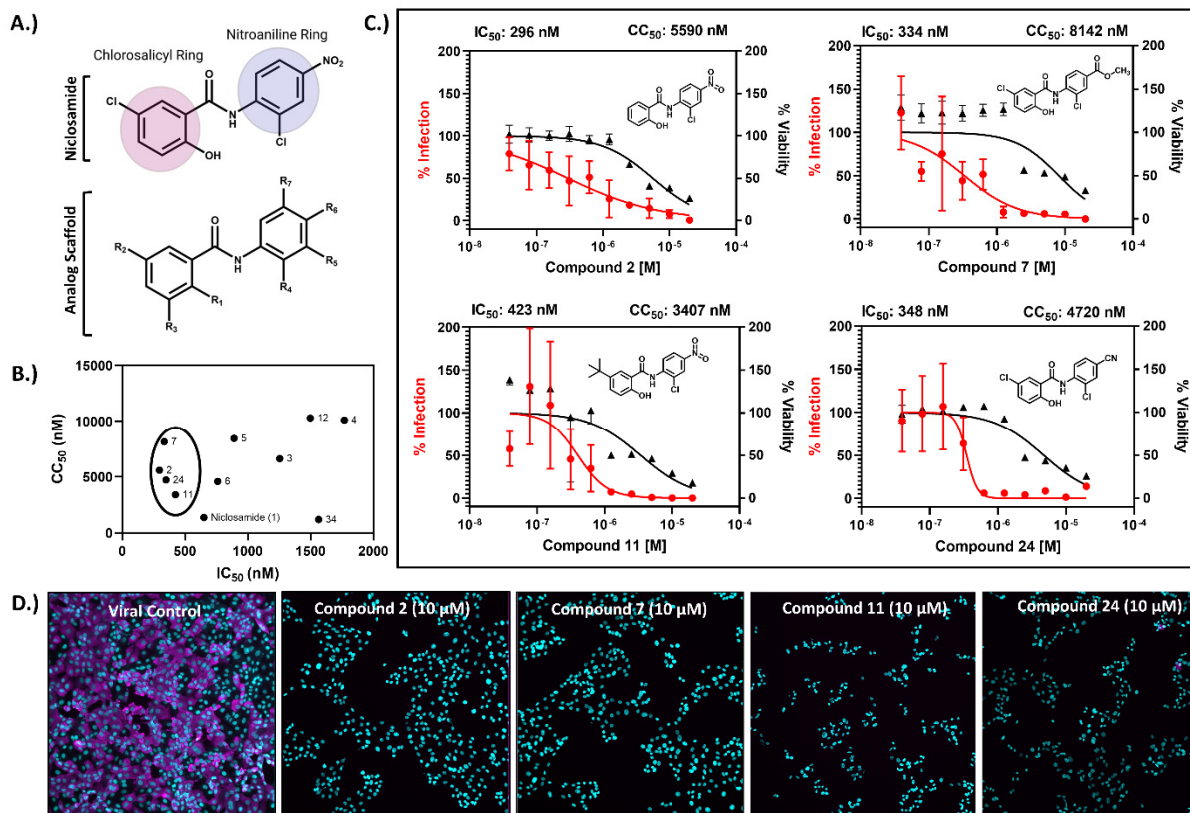
Figure 4. Niclosamide analogs have improved efficacy and reduced cytotoxicity in VeroE6.

A.) Structure of niclosamide indicating the chlorosalicyl/nitroaniline rings, and analog scaffold with modified substituent positions labeled. B.) IC_{50} vs. CC_{50} plot highlighting efficacious compounds in VeroE6. Compounds with improved potency and cytotoxicity profiles are circled on the plot. C.) 10-point, 2-fold concentration-response curves for the top four niclosamide analogs with a starting concentration of 20μM. Data are shown as the mean ± SEM of N=3 replicate wells per condition. Curves for infection (in red) and cell viability (in black) are included. D.) Representative images of infected cells treated with indicated compounds and viral control (Vehicle). (10X magnification, Cyan = nuclei, magenta = SARS-CoV-2 nucleocapsid protein).
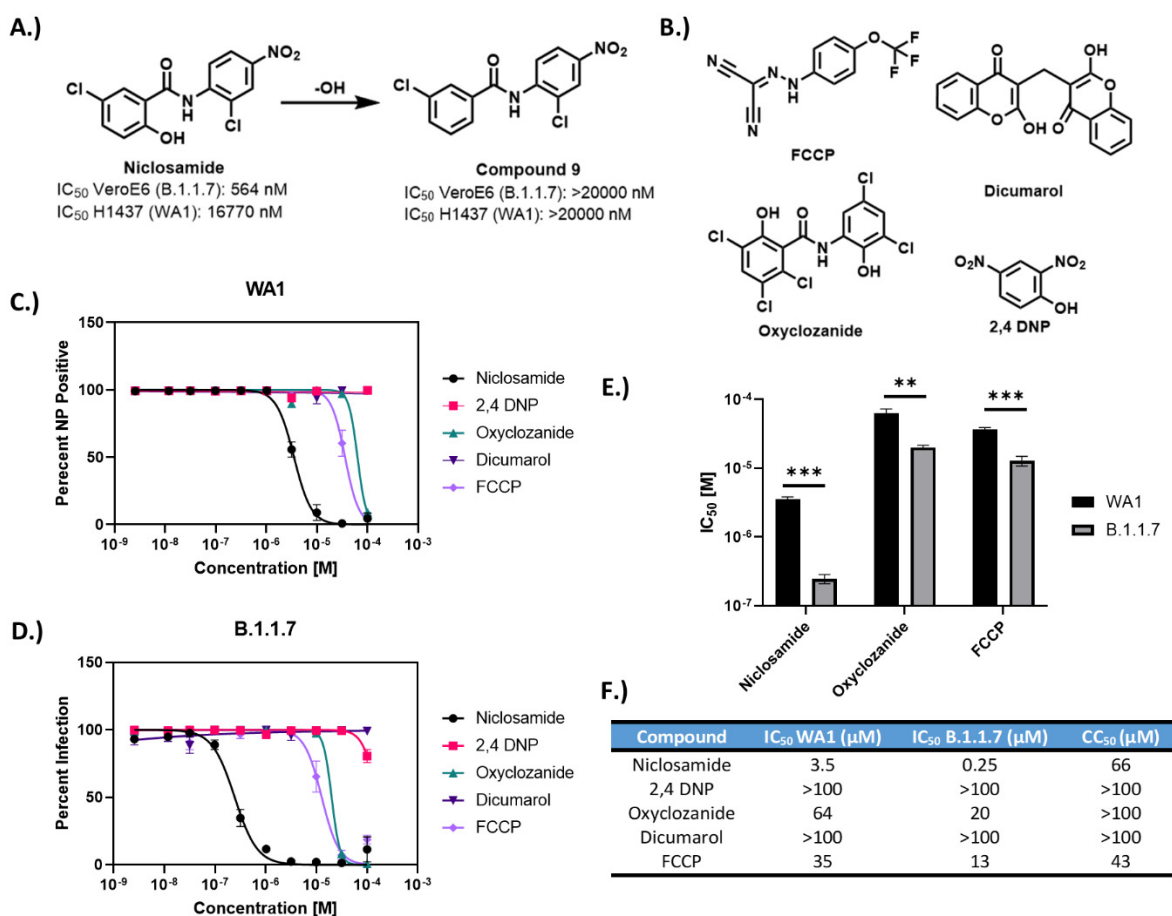
Figure 5. Efficacy of protonophores against SARS-CoV-2. A.) Removal of protonophore hydroxyl of niclosamide results in a complete loss of efficacy in both VeroE6 and H1437 cells. B.) Chemical structures for other protonophores evaluated against SARS-CoV-2 infection. C-D.) 10-point, 2-fold concentration response curves for protonophores versus WA1 variant (C.) and B.1.1.7 variant (D.) with starting concentrations of 100 μM. E.) IC_{50} plot for antiviral protonophores indicating significantly different potency against variants. F.) Table of IC_{50} and CC_{50} values for protonophores.
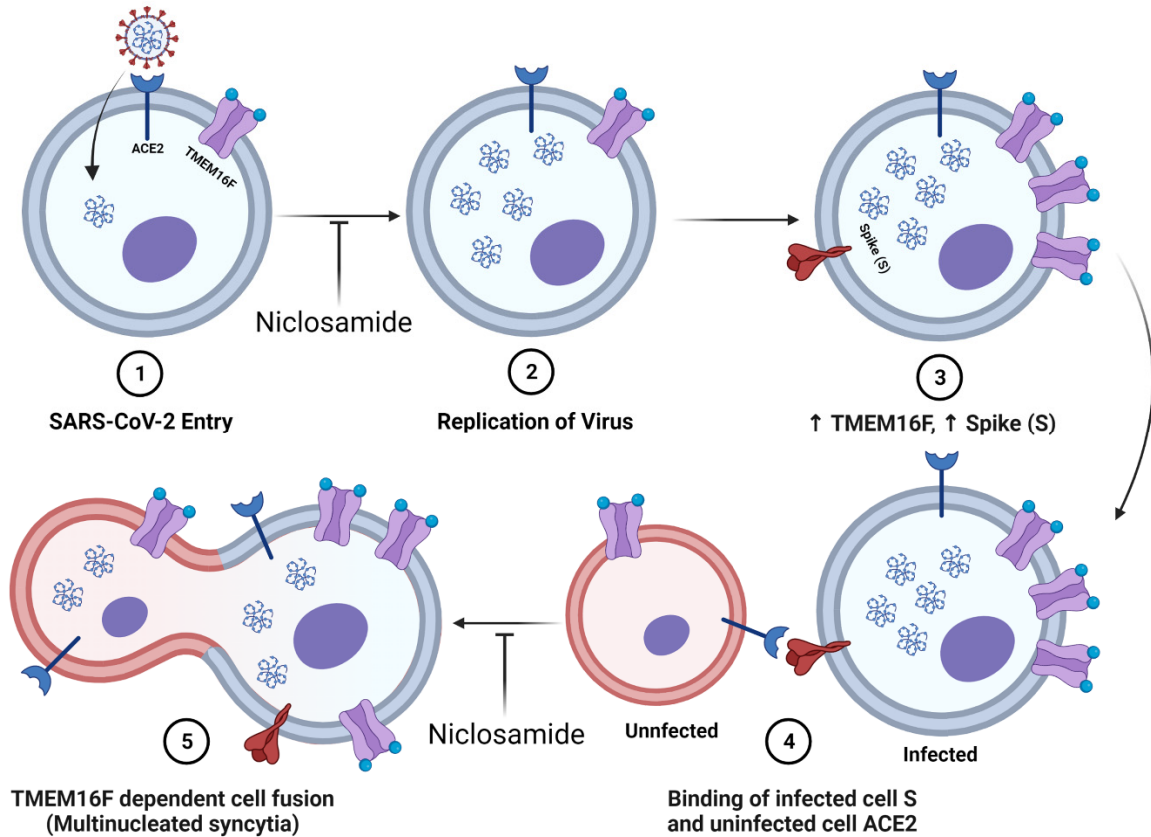
Figure 6. Diagram of niclosamides effect on SARS-CoV-2 entry and spike protein-mediated syncytia formation. 1.) SARS-CoV-2 binds to the ACE2 receptor of the host cell and enters. Niclosamide has been shown to inhibit this entry step *in vitro* 2.) Viral replication generates many copies of the RNA genome. 3.) Infection results in an increased expression of viral spike (S) protein and host cell TMEM16F at the plasma membrane. 4.) The S protein at the surface on an infected cell binds to the ACE2 receptor of an adjacent uninfected cell. 5.) Spike-dependent syncytia formation is mediated by the calcium-dependent lipid scramblase TMEM16F to generate multinucleated infected cell bodies. Niclosamide, an inhibitor of TMEM16F, has been shown to block spike-dependent syncytia formation.

Tables

Table 1. SAR table for Niclosamide Analogs. IC_{50} and CC_{50} values for VeroE6 (SARS-CoV-2 B.1.1.7 variant) and H1437 (SARS-CoV-2 WA1 variant). Physical properties including cLogP, pKa and logS were calculated using MOE and included in the table for each compound. Compounds that have efficacy against both cell lines are highlighted in gray.

Compound #	R1	R2	R3	R4	R5	R6	R7	Vero-E6 (B.1.1.7) IC$_{50}$ (nM)	CC$_{50}$ (nM)	H1437 (WA1) IC$_{50}$ (nM)	CC$_{50}$ (nM)	cLogP	pKa	logS
1 (Niclosamide)	OH	Cl	H	Cl	H	NO2	H	564	1050	16770	17060	4.17	7.98	-5.00
2	OH	H	H	Cl	H	NO2	H	296	5590	4915	8403	3.47	7.52	-4.32
3	OH	CH3	H	Cl	H	NO2	H	1254	6277	2595	3056	3.97	7.52	-4.66
4	OH	OCH3	H	Cl	H	NO2	H	1769	10110	10880	8941	3.39	7.65	-4.39
5	OH	Cl	H	Cl	H	H	H	890	8435	>20000	18570	4.17	8.01	-4.54
6	OH	Cl	H	Cl	H	CH3	H	760	4591	>20000	6048	4.66	8.01	-4.88
7	OH	Cl	H	Cl	H	COOCH3	H	334	8142	Inverted	>20000	4.15	7.98	-4.94
8	OH	Cl	H	Cl	H	COOH	H	>20000	>20000	Inverted	>20000	3.67	4.03	-4.54
9	H	Cl	H	Cl	H	NO2	H	>20000	>20000	>20000	>20000	4.63	14	-5.27
10	OH	Cl	H	Cl	H	OCH3	H	4248	>20000	Inverted	18900	4.05	8.02	-4.59
11	OH	t-Bu	H	Cl	H	NO2	H	423	3407	3097	1921	5.50	7.51	-5.68
12	OH	OCH3	H	Cl	H	NO2	H	1498	10290	16880	7529	3.39	7.65	-4.39
13	OH	t-Bu	H	Cl	H	COOCH3	H	>20000	14570	>20000	>20000	5.49	7.50	-5.62
14	OH	t-Bu	H	Cl	H	COOH	H	>20000	14250	Inverted	>20000	5.00	4.93	-5.22
15	OH	t-Bu	H	F	H	COOH	H	>20000	>20000	Inverted	>20000	4.41	4.73	-4.69
16	OH	t-Bu	H	CH3	H	COOH	H	>20000	>20000	Inverted	>20000	4.49	4.95	-4.74
17	OH	t-Bu	H	Cl	H	H	COOH	>20000	>20000	Inverted	>20000	5.00	4.93	-5.22
18	OH	t-Bu	t-Bu	Cl	H	CH3SO2N	H	>20000	>20000	Inverted	>20000	5.98	7.02	-6.39
19	OH	t-Bu	t-Bu	Cl	H	NH2	H	>20000	17590	Inverted	>20000	6.58	7.57	-6.14
20	OH	t-Bu	t-Bu	H	CH3	COOH	H	>20000	>20000	>20000	>20000	6.52	4.96	-6.10
21	OH	Cy	H	Cl	H	COOCH3	H	9910	>20000	>20000	>20000	5.96	7.50	-6.66
22	OH	Cy	H	Cl	H	COOH	H	4511	>20000	Inverted	>20000	5.48	4.93	-6.26
23	OH	CF3	H	CH3	H	COOCH3	H	>20000	>20000	>20000	>20000	4.97	7.49	-5.15
24	OH	Cl	H	Cl	H	CN	H	348	4720	1070	880	4.27	8.00	-5.03
25	OH	H	t-Bu	Cl	H	COOCH3	H	>20000	>20000	Inverted	>20000	5.22	7.52	-5.52
26	OH	t-Bu	t-Bu	Cl	H	COOH	H	>20000	>20000	>20000	>20000	6.77	4.93	-6.48
27	OH	t-Bu	t-Bu	Cl	H	COOCH3	H	16500	>20000	>20000	>20000	6.52	4.96	-6.10
28	OH	OCH3	H	CH3	H	COOH	H	>20000	>20000	Inverted	>20000	2.38	4.95	-3.46
29	OH	H	t-Bu	Cl	H	COOCH3	H	>20000	>20000	Inverted	>20000	5.22	7.52	-5.52
30	OH	H	t-Bu	Cl	H	COOH	H	>20000	>20000	Inverted	>20000	4.74	4.93	-5.12
31	OH	H	t-Bu	Cl	H	NO2	H	>20000	7214	>20000	1110	5.24	7.52	-5.58
32	OH	H	t-Bu	Cl	H	NH2	H	>20000	>20000	>20000	>20000	4.55	7.58	-4.78
33	OH	H	t-Bu	Cl	H	NSO2CH3	H	2879	>20000	Inverted	>20000	3.95	7.03	-5.03
34	OH	Cl	H	Cl	H	Br	H	760	5473	3491	3620	4.97	8.01	-5.36